Journal of Food Engineering 306 (2021) 110633

Contents lists available at ScienceDirect

Journal of Food Engineering

journal homepage: http://www.elsevier.com/locate/jfoodeng

Computer vision techniques on magnetic resonance images for the non-destructive classification and quality prediction of chicken breasts affected by the White-Striping myopathy

L. Carvalho [a], T. Pérez-Palacios [b], D. Caballero [c], T. Antequera [b], M.S. Madruga [a], M. Estévez [b,*]

[a] Postgraduate Program in Food Science and Technology, Department of Food Engineering, Federal University of Paraíba, João Pessoa, Paraíba, Brazil
[b] Institute of Meat and Meat Products (IPROCAR), TECAL Research Group, University of Extremadura, Cáceres, Spain
[c] Institute of Meat and Meat Products (IPROCAR), Media Engineering Group (GIM), University of Extremadura, Cáceres, Spain

ARTICLE INFO

Keywords:
Chicken breast
White-striping
Classification
MRI
Meat quality
Non-destructive technology

ABSTRACT

This study was designed to assess the capability of MRI-computer vision algorithms, as a non-destructive technique, to classify and predict quality characteristics of chicken breast affected by White-Striping (WS) myopathy. Samples showing moderate and severe degrees of the myopathy were analyzed together with normal samples (no WS symptoms). The influence of the computational algorithms to analyze the MRI images and the techniques of data analysis on the classification and prediction results was aimed. Computational features from both texture (GLCM) and fractal (OPFTA) algorithms were useful to i) classify WS chicken breast by means of different classification technique, Principal Component Analysis and Decision Tree, and ii) predict physico-chemical characteristics of these chicken breast with high accuracy, applying Multiple Linear Regression. The results show the feasibility of objectively classifying chicken breasts without sample destruction into two degrees of severity. This is of remarkable relevance in large processing plants where WS incidence is high and a quick decision-making is required for the fate of affected samples.

1. Introduction

White Striping (WS) is a clinical disorder that mainly affects the breast muscles of modern broiler and turkey strains (Soglia et al., 2018). This condition is characterized by the presence of white striation following the same direction of the muscle fibers (Petracci and Cavani, 2012). The occurrence of stretch marks in poultry breasts is associated with the current intensive and fast animal production systems. In an attempt to optimize meat production, human intervention in genetic selection, feeding and management of birds, has seriously affected chickens' physiology and eventually, meat quality (Petracci et al., 2019).

A fast body weight gain in broilers results in a remarkable increase of the breast muscle size that may lead to drastic histopathological changes, such as the necrosis and lyses of the fibers, inflammatory cell infiltration, vacuolar and hyaline degeneration and replacement of muscle damaged with connective tissue (fibrosis) and adipocytes (lipidosis) (Baldi et al., 2018; Kuttappan et al., 2013). As a consequence, there is a loss of nutritional and technological value of chicken meat affected by WS myopathy. Compared to meat from animals unaffected by the myopathy, WS meat commonly contains higher lipid and lower protein content (Baldi et al., 2018; Soglia et al., 2016) and display impaired water holding capacity (WHC) during cooking (Alnahhas et al., 2016; Petracci et al., 2013).

The identification of WS myopathy is usually performed by visual examination of the *Pectoralis major* muscle (Kuttappan et al., 2013). However, this traditional detection technique has some limitations as it requires a high number of trained evaluators and may be affected by the abilities of each individual (Geronimo et al., 2019). Although visual examination is the traditional and most widely used method for identification of WS meats, other non-destructive techniques have been studied to increase objectivity and accuracy. On this regard, the application of radiofrequency spectra (Traffano-Schiffo et al., 2017), image acquisition and computer vision system (Kato et al., 2019) and visible and near-infrared hyperspectral imaging (Jiang et al., 2019) presented successful results for the classification of WS samples.

Magnetic Resonance Imaging (MRI) has been widely used for food evaluation, as it is an innocuous, non-invasive, non-ionizing technique

* Corresponding author. Institute of Meat and Meat Products (IPROCAR), University of Extremadura, Avd. Universidad, sn. 10003, Cáceres, Spain.
E-mail address: mariovet@unex.es (M. Estévez).

https://doi.org/10.1016/j.jfoodeng.2021.110633
Received 18 January 2021; Received in revised form 7 April 2021; Accepted 7 April 2021
Available online 11 April 2021

and it does not require the destruction of the samples (Bonny et al., 2000; Ebrahimnejad et al., 2018). The application of MRI in foods is based on the fact that differences in the chemical properties of samples can generate differences in the absorption and emission of energy in the electromagnetic spectrum (Xiong et al., 2017). Several studies have been made in order to evaluate the quality characteristics of meat and meat products by MRI, allowing to prove the efficiency of this technique in predicting of moisture, salt, water activity (Torres et al., 2019), weight, lipid content (Pérez-Palacios et al., 2014) and sensory attributes (Caballero et al., 2018a), monitoring the quality of hams during the ripening process (Antequera et al., 2007), and in the classification of different samples (Pérez-Palacios et al., 2011). These goals were achieved by means of MRI in combination to computer vision algorithms and data mining techniques, to analyze the MRI images and the obtained data, respectively. In most of these studies, computational texture feature algorithms have been mainly applied for the analysis of MRI. Nowadays, the analysis of MRI with fractal algorithms is taking interest, because the classical texture algorithms seeks to compress image information while the use of fractals allows the identification of recurring patterns, removing the possibility of image compression (Caballero et al., 2018a).

Davanel et al. (2000) have applied MRI on chickens, to estimate the volume and the size of the carcasses and breasts, but, among the scientific literature, no more studies have been found focused on the use of MRI to classify chicken samples and/or determined the quality characteristics of this type of meat and/or its derived meat products.

This study firstly aims the objective and non-destructive classification and quality prediction of WS breast meat by means of MRI – computer vision algorithms – data mining techniques. The influence of the computational algorithms to analyze the MRI images and the techniques of data analysis on the classification and prediction results is also aimed.

2. Material and methods

2.1. Samples, identification and classification

For the present study, chicken breasts were purchased at four local supermarkets in Caceres, Spain. Samples were allocated to one of the following three groups based on the criteria described by Kuttappan et al. (2012): Normal ([N] did not show white striation on breast surface), WS-moderate ([WS-M] exhibited white striations with <1 mm thickness), and WS-severe ([WS-S] exhibited white striations with >1 mm thickness). Sixty chicken breasts ($n = 20$ of each type) were collected and used for the present study.

2.2. Physico-chemical properties

Protein, moisture, ash and collagen contents were analyzed in Normal, WS-moderate and WS-severe meats, according to the Association of Official Analytical Chemists (AOAC, 2000; ref. 923.03 ref. 935.29, ref. 971.19 and ref. 981.10, respectively). The fat content was determined according to the methodology described by Folch et al. (1957). pH was determined by direct electrode insertion on the cranial surface of each *Pectoralis major* muscle using a meat pH meter system (HI 99163, Hanna Instruments, Woonsocket, Rhode Island, USA). Color was measured in three different areas at the dorsal surface of the breast muscle using a Minolta colorimeter (Chroma Meter CR-300, Minolta Co., Osaka, Japan) in the CIELAB system (L* = lightness; a* = redness, and b* = yellowness) according to Carvalho et al. (2018). WHC was measured as percentage of cooking loss as described by Carvalho et al. (2018). Texture profile analysis (TPA) was performed in raw meat samples cut into parallelepiped (perpendicular to the muscle surface) with dimensions of 25 × 25 × 10 mm (length x width x thickness, respectively) and analyzed on a texturemeter (TA.TXplus texturemeter, Stable Micro Systems, Godalming, Surrey, UK). The samples were compressed twice to 50% of their original height with compression flat cylindrical aluminum probe (50 mm diameter) at a test-speed of 50 mm/min. The results were expressed in Newtons (N).

2.3. Oxidative stability

Lipid oxidation was determined in breast meat by the thiobarbituric acid-reactive substances (TBARS) assay using the method of Ganhão, Estévez & Morcuende (2011). The results from the samples were plotted against a standard curve prepared with known concentrations of tetraethoxypropane (TEP). The results were expressed as mg malondialdehyde (MDA) kg^{-1} breast meat. Protein oxidation was assessed through the quantification of total protein carbonyls using dinitrophenylhydrazine as described by Armenteros et al. (2009). The results were expressed as nmol carbonyls/mg protein.

2.4. MRI analysis

2.4.1. Image acquisition

MRI images were generated at the "Animal Source Foodstuffs Innovation Services" (SiPA) of the University of Extremadura (Cáceres, Spain). A low field MRI scanner (ESAOTE VET-MR E-SCAN XQ 0.18 T) with a hand/wrist coil was used. Each chicken breast (length: 178 ± 9 mm; width: 91 ± 5 mm; height: 24 ± 3 mm) was scanned one at a time. The Spin Echo (SE) T1-weighted sequence was used. The following parameters were used: field of view (FOV): 150 × 150 mm; echo time (TE): 26 ms; slice thickness: 4 mm; flip angle: 90°; repetition time (TR): 630 ms; matrix size: 256 × 204; phase encode: 204; number of acquisition: five per sample. The MRI acquisition was done at 23 °C. All the images were in DICOM format, with a 256 × 256 resolution, and 256 gray levels. Eleven slices per chicken breast were obtained across, and the acquisition took 30 min for each sample.

2.4.2. Image analysis

Once the MRI images of the chicken breast were obtained, they were analyzed by two computer vision algorithms, one based on texture (Gray Level Co-occurrence Matrix -GLCM-) (Haralick and Shapiro, 1993) and the other based on fractal (One Point of Fractal curve Texture Algorithm -OPFTA-) (Caballero et al., 2018b). The application of these algorithms allows extracting values for several features of the MRI images. In this way, numerical data are obtained from the images.

In the case of GLCM, firstly, the maximum rectangular area was selected in the image (Molano et al., 2012). Then, the selected areas were analyzed by applying the computational texture algorithm GLCM. It was computed by counting the number of times that each pair of gray levels occurs at a given distance d and for all directions. In this matrix, each item $p(i, j)$ denotes the times that two neighboring pixels separated by distance d occur on the image, one with gray level i and the other with gray level j. In this way, GLCM was constructed with information of the complete ROI and includes 10 features: ENE (energy), ENT (entropy), COR (correlation), HC (Haralick's correlation), IDM (inverse difference moment), INE (inertia), CS (cluster shade), CP (cluster prominence), CON (contrast), and DIS (dissimilarity) (Haralick and Shapiro, 1993).

The fractal algorithm, OPFTA, (Caballero et al., 2018b), is a novel texture algorithm based on features obtained from fractal values. Before applying this algorithm, the largest area rectangle inscribed in the contour of the chicken was also selected (Molano et al., 2012). Later, each rectangle was divided into smaller rectangles of 32 × 32 pixels, so called, region of interests (ROI). Then, a two-dimensional variation of the Minkowski-Bouligand algorithm (Mandelbrot, 1982) was applied on each ROI in order to achieve the local exponents with the different box sizes (powers of 2). From all local exponent, the local exponent with the box size equal to eight was selected, this is the most representative one (Caballero et al., 2018b). After that, a matrix with the values of the most representative local exponent of each ROI was gathered. Finally, seven texture features were computed on each matrix: Uniformity (UNI), Entropy (ENT), Correlation (COR), Homogeneity (HOM), Inertia (INE),

Contrast (CON) and Efficiency (EFI) (Aggarwal and Agrawal, 2012).

2.4.3. Data mining analyses

The free software WEKA (Waikato Environment for Knowledge Analysis) (http://cs.waikato.ac.nz/ml/weka - last accessed: September 2020) was used to carry out the classification and predictive techniques of data mining. The advantages of using data mining tools as WEKA is that calibration and validation are achieved by using the same data sets, not being necessary to perform the validation with a different data set, allowing the development of the prediction model (Caballero et al., 2016a).

2.4.3.1. Classification techniques. A classical Principal Component Analysis (PCA) (Bro and Smilde, 2014) was applied to evaluate the distribution of samples. This technique also analyses the relationships between the computational texture characteristics obtained and the physico-chemical parameters of the groups of samples.

The J48 decision tree (DT) algorithm was also applied as classification technique in this study. DT is a decision modelling tool that graphically displays the classification process of a given input for given output class labels (Safavian and Landgrebe, 1991). This method is one of the learning algorithms that generate classification models in the form of a tree structure. It is based on the "divide and conquer" strategy (Safavian and Landgrebe, 1991). Data subsets were created by decomposing the whole dataset into smaller datasets. The final model is a tree structure with decision and leaf nodes.

A confidence factor of 0.5 and minimum bucket size of 3 were applied (Safavian and Landgrebe, 1991), being the bucket size, the minimum number of samples that can be classified in any leaf of the DT.

The statistical assessment of the classification performance can be carried out by using different classifiers (Demsar, 2006; Hand, 2012). In our case, the model was statistically evaluated by using the sensitivity (SENS), specificity (SPEC), positive predictive value (PPV), negative predictive value (NPV), error rate, fall-out rate, false discovery rate (FDR), false omission rate (FOR), the critical success index (CSI), the accuracy and the F1 score. These parameters are given by the following equations:

$$SENS = \frac{TP}{TP + FN}$$

$$SPEC = \frac{TN}{FP + TN}$$

$$PPV = \frac{TP}{TP + FP}$$

$$NPV = \frac{TN}{TN + FN}$$

$$Error\ rate = \frac{FN}{TP + FN}$$

$$Fall\ out\ rate = \frac{FP}{FP + TN}$$

$$FDR = \frac{FP}{TP + FP}$$

$$FOR = \frac{FN}{TN + FN}$$

$$CSI = \frac{TP}{TP + FN + FP}$$

$$Accuracy = \frac{TP + TN}{TP + TN + FP + FN}$$

$$F1\ Score = \frac{2 \cdot TP}{2 \cdot TP + FP + FN}$$

where, TP and TN stand for True Positive and True Negative, respectively, accounting for the samples that have been correctly assigned as belonging (TP) or not belonging (TN) to a specific class. FP and FN stand for False Positive and False Negative, respectively, accounting for the samples that have been wrongly assigned as belonging (FP) or not belonging (FN), to a specific class.

2.5. Prediction techniques

Predictive techniques allow creating future models that can be predicted from current data by trend analysis (Witten and Frank, 2005; Wu et al., 2008).

Multiple Linear Regression (MLR) is used to represent linear relationship between a dependent variable and several independent variables. This technique obtains a linear regression equation, which can be used to predict future values (Hastie et al., 2001).

$$y = \omega_0 + \sum_{1}^{n} \omega_i x_i$$

The M5 method of attribute selection was applied in our experiments. This method steps through the attributes removing the one with the smallest standardized coefficient until no improvement is observed in the estimation of the error (Kira and Rendell, 1992). A ridge value of 1.0×10^{-4} was applied too. The estimation procedure was 10-fold cross validation, where the data is divided into 10 partitions of equal size. One subset is tested each time and the remaining data are used for fitting the model. The process is repeated sequentially until all subset have been tested. Therefore, all data are used for training and testing. However, although this method requires 10 repetition analysis, this is a robust method (Dietterich, 1998).

Isotonic Regression (IR) provides a set of values from the information stored on a database. It is based on estimating the ordered values for an independent variable as a function of one of the input parameters. Only the input parameters providing better adjustment results will be selected. Finally, an interpolation was established (polynomial trend line) to compare the predicted data set with the original values in the database, obtaining the prediction equation (Barlow et al., 1972).

$$y = \sum_{0}^{n} \omega_i x^i$$

The correlation coefficient (r) was used to evaluate the goodness of fit the prediction and for its validation, according to the rules given by Colton (1974). This author considered r from 0 to 0.25 as little to no relationship; from 0.25 to 0.50 indicates a weak degree of relationship; from 0.50 to 0.75, indicates a moderate to good relationship and from 0.75 to 1 indicates a very good to excellent relationship.

$$r = \sqrt{\frac{\sum_{i=1}^{n} (f_i - \bar{y})^2}{\sum_{i=1}^{n} (y_i - \bar{y})^2}}$$

where f_i is the predicted value, y_i is the real value and $\bar{y}$ is the average value.

The mean absolute error (MAE) and weighted absolute percentage error (WAPE) were used to evaluate the prediction results too (Ávila et al., 2019). The MAE measures the difference between real and predicted values and WAPE measures the same difference but expressed as a percentage of the attribute mean. They are given by the following equations:

$$MAE = \frac{1}{n} \sum_{i=1}^{n} |f_i - y_i|$$

Table 1
Chemical and physical properties of normal chicken breast (N) and those affected by the white striping myopathy in the moderate (WS-M) and severe (WS–S) degrees (mean ± standard deviation).

	N	WS-M	WS-S	*p* value
Moisture[A]	75.75 ± 0.66	75.70 ± 1.04	75.75 ± 1.07	0.989
Proteins[A]	21.65^{a} ±0.70	20.65^{b} ± 1.00	20.28^{b} ± 0.83	0.004
Lipids[A]	2.56^{b} ± 0.54	4.03^{a} ±0.66	4.10^{a} ±0.81	<0.001
Ash[A]	1.06 ± 0.09	1.01 ± 0.11	1.11 ± 0.10	0.175
Collagen[A]	0.38^{b} ± 0.03	0.49^{a} ±0.11	0.48^{a} ±0.06	0.008
pH	5.60b ± 0.18	5.92a±0.18	5.88^{a} ±0.15	<0.001
Color L*	60.55^{a}±1.87	58.24^{ab} ± 2.16	58.09^{b} ± 2.24	0.025
Color a*	0.70^{b} ± 0.25	0.72^{b} ± 0.31	2.25^{a} ±0.76	0.030
Color b*	7.21^{a} ±2.40	7.93^{a} ±1.99	5.29^{b} ± 1.96	0.041
Hardness[B]	63.46^{c}±8.98	98.10^{a} ±10.58	71.80^{b} ± 7.51	0.024
Adhesiveness[C]	−0.25 ± 0.06	−0.22 ± 0.04	−0.24 ± 0.07	0.473
Springiness[D]	0.79^{ab} ± 0.08	0.76^{b} ± 0.11	0.88^{a}±0.03	0.014
Cohesiviness[E]	0.64 ± 0.05	0.60 ± 0.11	0.59 ± 0.04	0.365
Gumminess[B]	41.21^{c}±8.56	74.58^{a} ±6.67	47.25^{b} ± 5.06	0.023
Chewiness[C]	37.82^{c}±7.54	65.25^{a} ±4.98	43.08^{b} ± 6.18	0.036
Resilience[E]	0.36 ± 0.09	0.39 ± 0.11	0.38 ± 0.03	0.758
TBARs[F]	0.22^{c} ±0.08	0.37^{b} ± 0.09	0.64^{a} ±0.19	0.018

Some of the results displayed in the present table were partially shown elsewhere (Carvalho et al., 2020).
[a-c] Mean values within the same parameter followed by different superscript letters significantly differ by the Tukey test ($p < 0.05$).
[A] Results expressed as g/100 g muscle.
[B] Results expressed as N/cm.^{2}.
[C] Results expressed as N x sec.
[D] Results expressed as cm.
[E] Results are dimensionless.
[F] Results expressed as mg MDA/kg muscle.

$$WAPE\ (\%) = \frac{100 \cdot \sum_{i=1}^{n} |f_i - y_i|}{\sum_{i=1}^{n} f_i}$$

where f_i is the predicted and y_i is the real value.

3. Results and discussion

3.1. Characterization of chicken breast

3.1.1. Physico-chemical analysis

The physico-chemical properties of N chicken breasts and those affected by the WS myopathy, are shown in Table 1. The WS myopathy was manifested as variations in the chemical composition, pH, color and texture properties and oxidative stability of chicken breasts. Total protein content was significantly lower in chicken breasts affected by the WS condition. This result is in line with previous reports and may be regarded as a reflection of the myodegeneration process that leads to a depletion of muscle proteins, and loss of several essential amino acids (Adabi and Soncu, 2019). The accretion of lipids and collagen is also a typical feature of the WS myopathy owing to the lipidosis and fibrosis processes (Petracci et al., 2019). These effects have also been observed in this study, with significant higher lipid and collagen percentages in N chicken breast than in WS ones. In chicken breasts affected by the WS condition, muscle tissue is replaced by degenerative lesions in which adipocytes and connective tissue are deposited (Petracci et al., 2019). WS breasts displayed higher final pH value than N counterparts which is a reflection of a reduced glycogen content or impaired post-mortem acidification process (Carvalho et al., 2017).

Instrumental color of chicken breasts was also significantly affected by the WS condition. WS-S muscles were darker (lower L^* values) than N breasts while WS-M displayed intermediate values. On the contrary, WS-S samples were redder (higher a^* values) than N chicken breasts. The b^* values (yellowness) were significantly lower in WS-S than in N and WS-M chicken breasts. These outcomes are consistent with those reported by other authors such as Petracci et al. (2013) or Kuttappan et al. (2017) who attributed these changes to the lipid accumulation (increased yellowness) and the occurrence of congestion and inflammation in the WS muscles (decreased lightness and increased redness).

In regards to the texture properties, overall, WS-M samples displayed the most affected profile as compared to N chicken breasts. Hardness and related parameters such as gumminess and chewiness were found to be higher in WS-M samples than in N samples while WS-S displayed intermediate values. These results could be ascribed to the increased fibrosis and greater collagen content in WS chicken breast. The decrease in hardness in the WS-S samples compared to the WS-M counterparts, already described elsewhere (Carvalho et al., 2020) was attributed to a severe protein degradation that in WS-S, could have a greater impact on texture properties than collagen accretion. Oxidative instability is actually a typical feature in chicken breasts affected by the WS myopathy (Petracci et al., 2019; Carvalho et al., 2020). In the present samples, in fact, the concentration of TBARS was affected by the WS conditions as a clear effect of the degree of severity was observed. As already

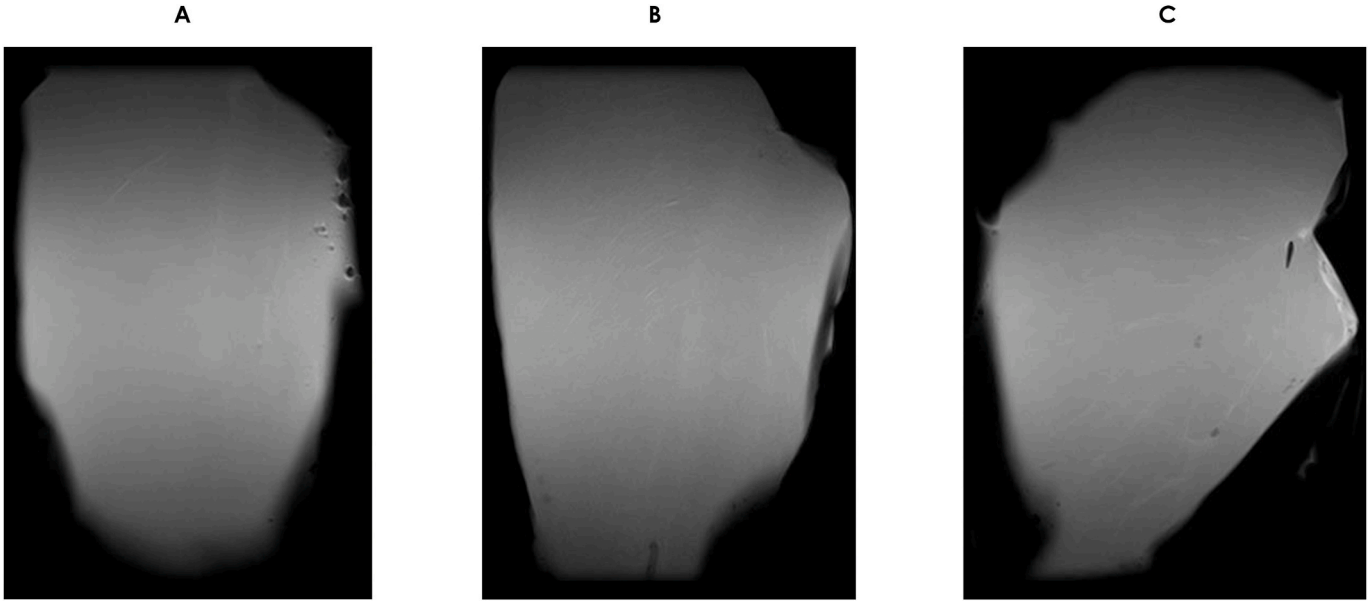

Fig. 1. MRI of normal chicken breast (A) and those affected by the white striping myopathy in the moderate (B) and severe (C) degrees.

Table 2
Average values of the computational features[A] from GLCM and OPFTA algorithms of MRI from normal chicken breast (N) and those affected by the white striping myopathy in the moderate (WS-M) and severe (WS–S) degrees.

		N	WS-M	WS-S	*p* value
GLCM	ENE	$0.23.10^{-2a} \pm 0.10.10^{-2}$	$0.25.10^{-2b} \pm 0.13.10^{-2}$	$0.30.10^{-2c} \pm 0.10.10^{-2}$	0.021
	ENT	2.53 ± 0.57	2.60 ± 0.42	2.66 ± 0.27	0.165
	COR	$0.10.10^{-2a} \pm 0.04.10^{-2}$	$0.15.10^{-2c} \pm 0.11.10^{-2}$	$0.13.10^{-2b} \pm 0.04.10^{-2}$	0.026
	HC	$14.77.10^{3b} \pm 41.72.10^{2}$	$15.06.10^{3c} \pm 53.09.10^{2}$	$13.71.10^{3a} \pm 18.00.10^{2}$	0.037
	IDM	$0.54^{b} \pm 0.11$	$0.51^{a} \pm 0.10$	$0.56^{c} \pm 0.05$	0.024
	INE	$6.37^{b} \pm 5.83$	$7.14^{c} \pm 5.86$	$3.78^{a} \pm 3.28$	0.048
	CS	$0.04.10^{-2} \pm 0.03.10^{-2}$	$0.06.10^{-2} \pm 0.05.10^{-2}$	$0.06.10^{-2} \pm 0.04.10^{-2}$	0.159
	CP	$4.47.10^{-6a} \pm 3.79.10^{-6}$	$9.74.10^{-6c} \pm 5.95.10^{-6}$	$5.94.10^{-6b} \pm 5.86.10^{-6}$	0.046
	CON	$0.20.10^{-2a} \pm 0.07.10^{-2}$	$0.26.10^{-2c} \pm 0.06.10^{-2}$	$0.23.10^{-2b} \pm 0.05.10^{-2}$	0.004
	DIS	$1.39^{b} \pm 0.66$	$1.48^{c} \pm 0.74$	$1.17^{a} \pm 0.27$	0.029
OPFTA	UNI	$495.79^{b} \pm 351.83$	$478.28^{a} \pm 295.80$	$605.87^{c} \pm 240.99$	0.039
	ENT	$58.95^{a} \pm 52.52$	$58.14^{a} \pm 42.60$	$76.87^{b} \pm 37.41$	0.037
	COR	$17.11.10^{2b} \pm 13.51.10^{2}$	$19.44.10^{2c} \pm 14.69.10^{2}$	$15.69.10^{2a} \pm 12.77.10^{2}$	0.029
	HOM	$36.87^{a} \pm 17.64$	$37.99^{a} \pm 19.96$	$48.57^{b} \pm 14.46$	0.009
	INE	$19.11.10^{3} \pm 17.23.10^{3}$	$16.52.10^{3} \pm 12.93.10^{3}$	$16.93.10^{3} \pm 10.59.10^{3}$	0.383
	CON	$33.80.10^{3c} \pm 32.65.10^{3}$	$28.87.10^{3a} \pm 22.15.10^{3}$	$31.09.10^{3b} \pm 19.79.10^{3}$	0.036
	EFI	$1.91^{b} \pm 1.08$	$1.46^{a} \pm 0.83$	$1.92^{b} \pm 0.86$	0.025

[a-c] Mean values within the same parameter followed by different superscript letters significantly differ by the Tukey test ($p < 0.05$).
[A] ENE: energy; ENT: entropy; COR: correlation; HC: Haralick's correlation; IDM: inverse difference moment; INE: inertia; CS: cluster shade; CP: cluster prominence; CON: contrast; DIS: dissimilarity; UNI: Uniformity; ENT: Entropy; COR: correlation; HOM: homogeneity; INE: inertia; CON: contrast; EFI: Efficiency.

discussed in a previous paper (Carvalho et al., 2020) this increased susceptibility of lipids from WS chicken breasts to suffer oxidative damage during subsequent processing could affect the sensory and nutritional value of chicken meat.

3.1.2. MRI analysis

Fig. 1 shows MRI images of the three types of chicken breasts under study: N (Fig. 1A), WS-M (Fig. 1B) and WS-S (Fig. 1C). Visual differences can be appreciated among the images of the different groups. The chicken meat color can be defined as light gray. In the case of WS batches, the MRI images show white and raised lines, being bigger and more evident in WS-S samples than in WS-M ones. However, these marks are not relevant in the N batch. These findings agree with the classification made following the criteria of Kuttappan et al. (2012). The white and raised lines observed in the MRI images of WS samples may be caused by the fibrosis and lipidosis that take place in chicken breast with this myopathy. Certainly, MRI acquisition by applying SE-T1 sequences allow the detection of hydrogen and other features like fat fluidity, which lengthen the T1 relaxation time (Lufkin, 1998). Thus, those effects influencing on lipids could modify T1 and lead to differing MRI. However, since fat has lower T1 values than muscle (around 90 vs around 450 ms, respectively) (Touissan et al., 2005), and chicken breast are very lean, the lipid signal is probably lower than those of lean in the samples of this study, with the fibrosis having a more plausible influence. In fact, in a previous study with cod fish, visual differences were appreciated in MRI from samples cooked at different temperatures, which was ascribed to denaturing collagen (Perez-Palacios et al., 2017a). This is supported by results exposed in Table 1, with WS samples having higher percentage of collagen than N ones. These findings point out the capability of MRI to visually identify breast chicken affected by WS, which agrees with the results obtained by Perez-Palacios et al. (2011) in hams. These authors were able to perform a visual distinction of Iberian hams from pigs with different feeding background by using MRI.

Table 2 shows the mean values of the computational texture features obtained from the MRI images of each type of breast chicken. Fourteen

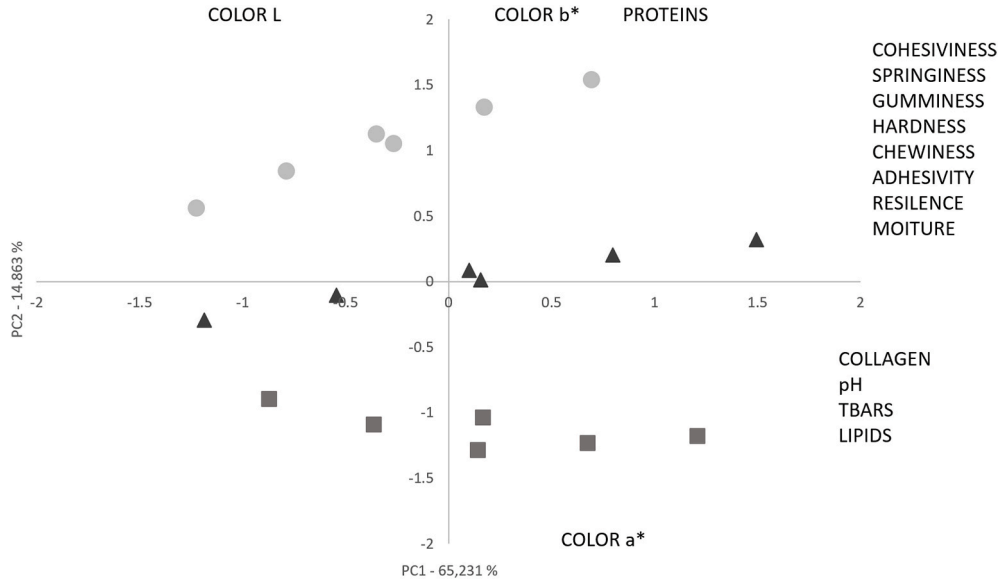

Fig. 2. Principal component analysis of physico-chemical parameters of normal chicken breast (●) and those affected by the white striping myopathy in the moderate (▲) and severe (■) degrees.

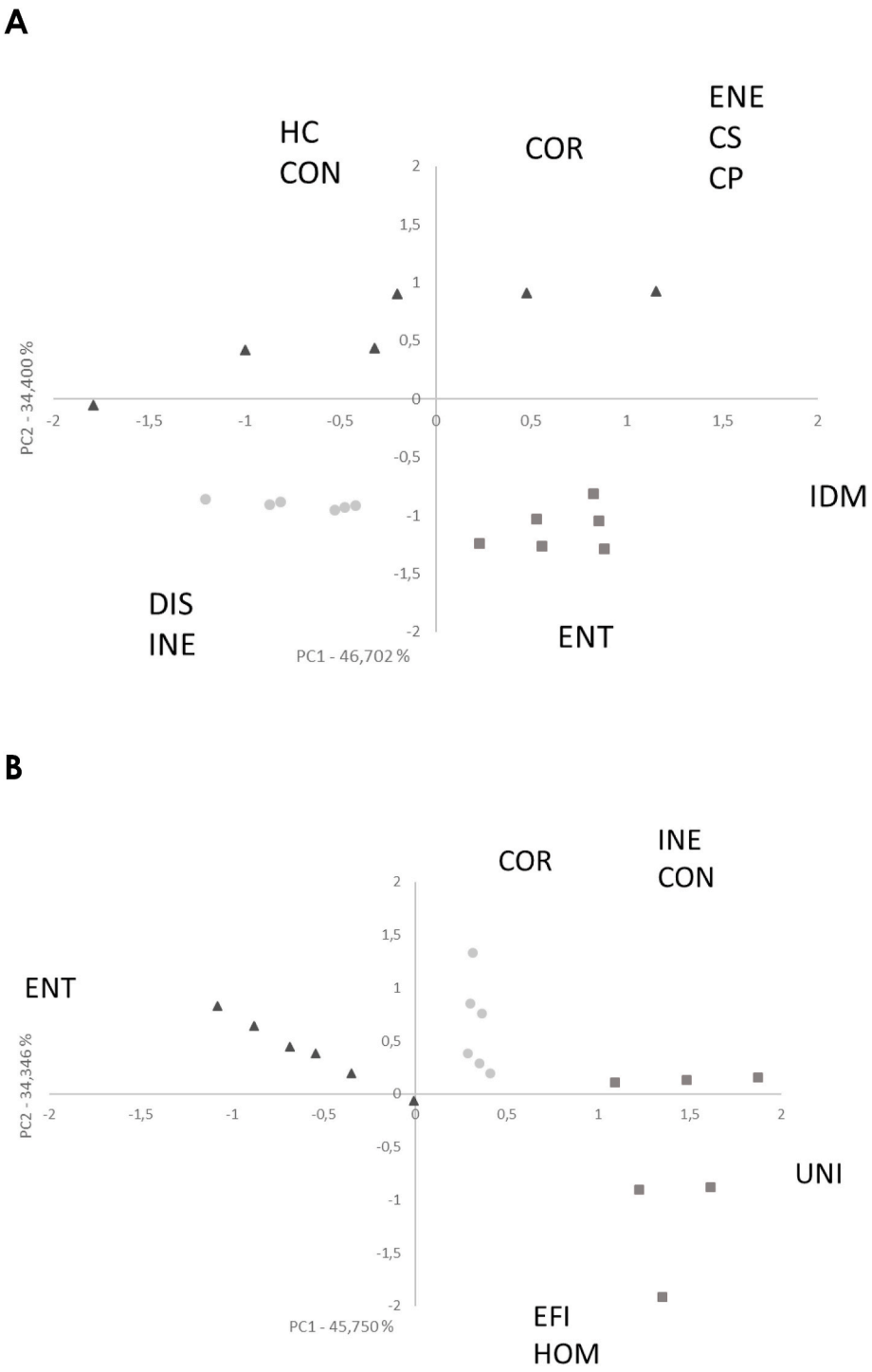

Fig. 3. Principal component analysis of GLCM (A) and OPFTA (B) computational characteristics from MRI of normal chicken breast (●) and those affected by the white striping myopathy in the moderate (▲) and severe (■) degrees.

(ENE, COR, HC, IDM, INE, CP, CON, DIS, UNI, ENT, COR, HOM, CON and EFI) of seventeen computational features showed statistical differences ($p < 0.05$) among groups. More specifically, in comparison to N and WS-M samples, WS-S ones obtained higher values for ENE, UNI, ENT, and HOM and lower for INE, DIS and COR; HC and CP were lower in N and WS-S than in WS-M chicken, while IDM, EFI and CON showed higher values in N and WS-S than in WS-M samples. The values of COR and CON were higher in WB samples than in C ones. Considering the meaning of the texture features (Ávila et al., 2015), WB-S chicken breasts can be described as quite uniform (high ENE), with a messy and complex texture (high ENT) a low difference in the gray levels (low INE and DIS), while WS-M samples could be characterized as not very homogeneous (low IDM) with scattered and symmetric gray levels (high HC and CP). Images of C samples are mainly characterized by a very low contrast (low CON). Previous studies have also noted significant differences in the computational characteristics of MRI from hams, loins and cod as affected by feeding, processing and cooking (Perez-Palacios et al., 2017a; Caballero et al., 2018a, 2018b).

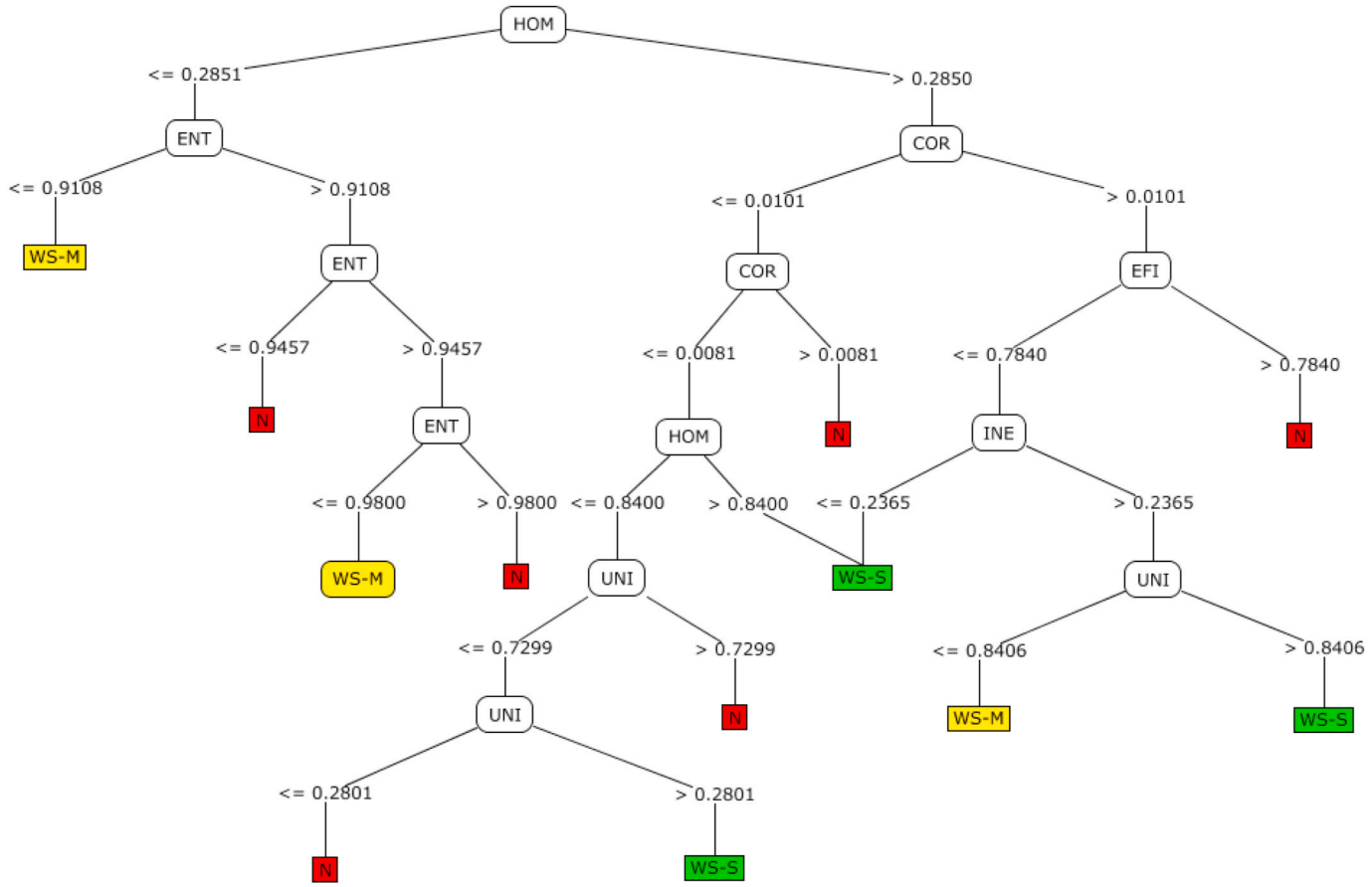

Fig. 4. Decision Tree classification model of normal chicken breast (N) and those affected by the white striping myopathy in the moderate (WS-M) and severe (WS–S) degrees based on the computational characteristics of the OPFTA algorithm.

3.2. Classification of chicken breast based on physico-chemical and MRI analysis

Fig. 2 exposes PCA of sample data as a function of the physico-chemical characteristics. The first two principal components (PC1 and PC2) accounted for 80.09% of the total variance (65.23% for PC1, and 14.86% for PC2) accumulating more than 65% recommended (Bro and Smilde, 2014). The score plot shows the three group of chicken breasts clearly separated. The N group of chicken breasts was in the two upper quadrants, and positively related to lightness (L*) and the percentage of proteins. In fact, the highest values for these parameters have been found in the N group of samples (Table 1). WS-S group of chicken breast was positioned in the two bottom quadrants, near to the percentage of lipids, redness (a^*) and TBARS, in concordance with results on Table 1 that shows the highest values for these physico-chemical characteristics in the WS-S samples. WS-M chicken breasts were found in the central part of the score plot and close to most analyzed texture parameters (hardness, adhesively, gumminess or resilience). This agrees with the highest values of these characteristics in the WS-M samples as compared to those from the other groups (Table 1).

Fig. 3 shows PCA biplots (variables and samples) of chicken breast samples affected by the WS condition as a function of MRI computational features from two computer vision algorithms, GLCM (Fig. 3A) and OPFTA (Fig. 3B).

Table 3
Results on classification of chicken breast with different affection of white striping myopathy by applying DT[a] as data mining technique.

		SENS[b]	SPEC[c]	PPV[d]	NPV[e]	ERROR RATE	FALL-OUT RATE	FDR[f]	FOR[g]	CSI[h]	ACCURACY	F1 SCORE
GLCM	N	0.9444	1	1	0.9730	0.0556	0	0	0.0270	0.9444	0.9815	1.8889
	WS-M	0.9444	0.9167	0.8500	0.9706	0.0556	0.0833	0.1500	0.0294	0.8095	0.9259	1.6190
	WS-S	0.8889	0.9722	0.9412	0.9459	0.1111	0.0278	0.0588	0.0540	0.8421	0.9444	1.6842
OPFTA	N	1	0.9722	0.9474	1	0	0.0278	0.0526	0	0.9474	0.9815	1.8947
	WS-M	0.8889	0.9167	0.8421	0.9429	0.1111	0.0833	0.1579	0.0571	0.7619	0.9074	1.5238
	WS-S	0.8333	0.9722	0.9375	0.9211	0.1667	0.0278	0.0625	0.0789	0.7895	0.9259	1.5789

[a] DT: Decision Tree.
[b] SENS: Sensitivity.
[c] SPEC: Specificity.
[d] PPV: Positive Predictive Value.
[e] NPV: Negative Predictive Value.
[f] FDR: False Discovery Rate.
[g] FOR: False Omission Rate.
[h] CSI: Critical Success Index.

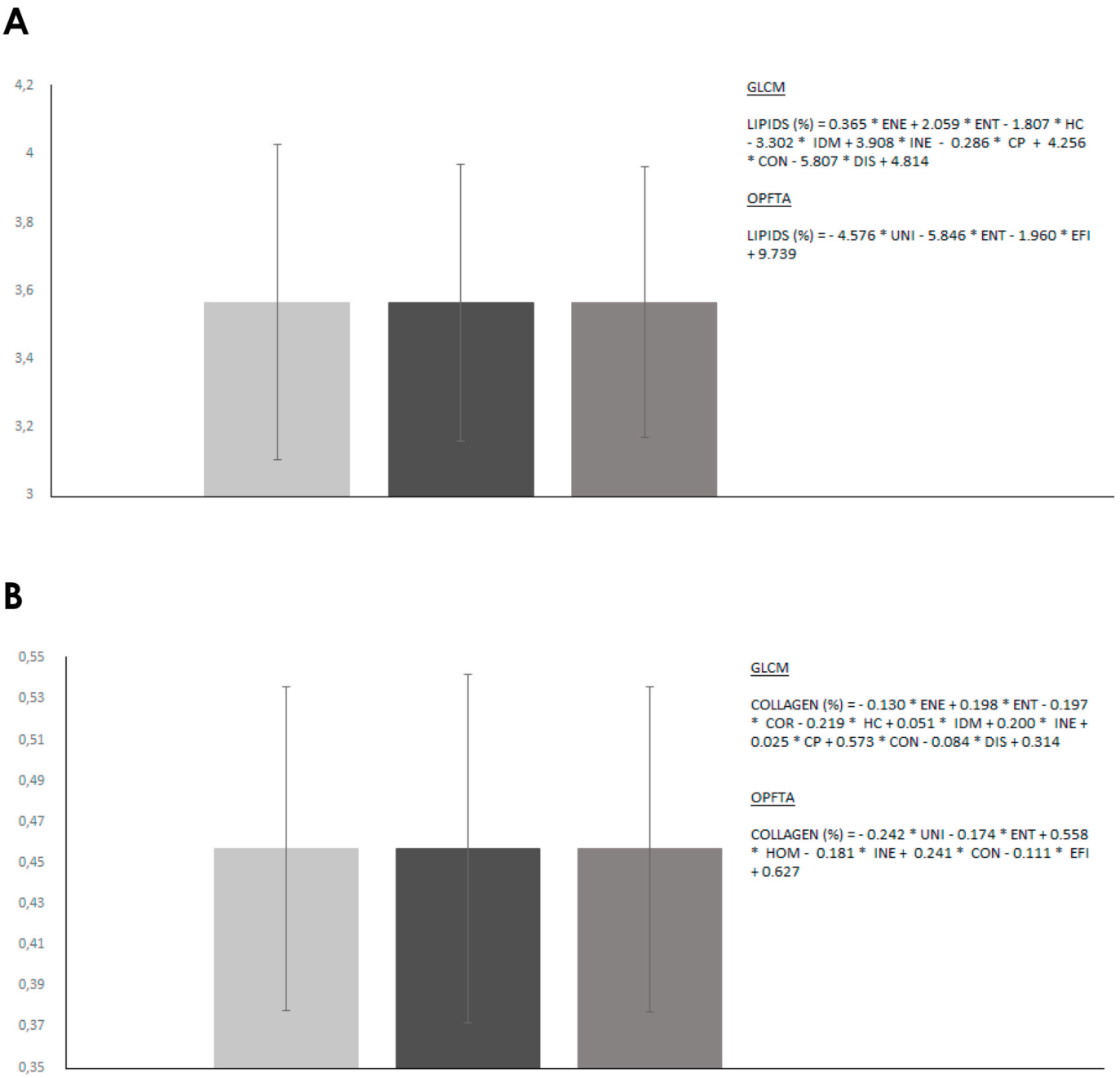

Fig. 5. Percentages of lipids (A) and collagen (B) determined by chemical analysis (■) and prediction equations as a function of computational characteristics* of GLCM (■) and OPFTA (■) algorithms.

As for GLCM results, the first two PC accounted for 81.10% of the total variance (46.70% for PC1, and 34.40% for PC2) accumulating more than 65% recommended (Bro and Smilde, 2014). Samples labelled as WS-M group (dark gray triangles) were correlated positively by PC1 and were associated to the ENE, COR, HC, CON, CS and CP computational features. Samples of the WS-S group (gray squares) were located on the right bottom quadrant and were related to the ENT and IDM computational features. The N group of samples (light gray circles) were positioned on the left bottom quadrant of the PCA and these samples were correlated to the INE and computational features. In the PCA on OPTFA results (Fig. 3B), the first two principal components accounted for 80.10% of the total variance (45.75% for PC1, and 34.35% for PC2) accumulating more than 65% recommended (Bro and Smilde, 2014). The group of samples labelled as WS-M (dark gray triangles) were correlated negatively by PC2 and were related to the ENT computational features. The N group of samples (light gray circles) were located at the right upper quadrant and were correlated to the COR, INE and CON computational features. The WS-S group (gray squares) were found in the right bottom quadrant of the PCA. These samples are related to UNI, HOM and EFI. Thus, MRI computational features of GLCM and OPTFA algorithms achieved separating chicken breasts with moderate and severe WS and without this clinical disorder.

In previous studies, the use of computational texture features from MRI of meat products also reached to classify meat products as a function of different variables. Cernadas et al. (2001), for example, classified dry-cured Iberian loins as a function of the genotypes of the pigs. Pérez-Palacios et al. discriminated fresh (Pérez-Palacios et al., 2011) and dry-cured (Pérez-Palacios et al., 2010) Iberian hams as a function of the feeding of the pigs.

Besides PCA, in this study, DT was also applied to evaluate the ability

Table 4
Correlation Coefficient (R), Mean Absolute Error (MAE) and Weighted Absolute Percent Error (WAPE) of the prediction equations of physico-chemical parameters of chicken breast as a function of two computational texture algorithms (GLCM and OPFTA) and two data mining technique (multiple linear regression (MLR) and isotonic regression (IR).

	GLCM						OPFTA					
	MLR			IR			MLR			IR		
	R	MAE	WAPE	R	MAE	WAPE	R	MAE	WAPE	R	MAE	WAPE
Hardness	0.8036	6.335	0.112	0.6612	10.677	0.189	0.8056	9.233	0.166	0.2461	9.991	0.180
Adhesivity	0.6582	18.170	0.078	0.6381	23.251	0.099	0.7998	15.295	0.065	0.3573	24.239	0.103
Springiness	0.8373	0.023	0.029	0.6608	0.067	0.084	0.8309	0.035	0.044	0.6411	0.059	0.074
Cohesiviness	0.8169	0.020	0.033	0.6021	0.053	0.077	0.8593	0.029	0.048	0.4356	0.066	0.089
Gumminess	0.8117	540.508	0.153	0.6526	980.747	0.227	0.8143	635.050	0.180	0.5321	855.755	0.243
Chewiness	0.8025	419.228	0.150	0.6392	770.759	0.276	0.8188	411.747	0.147	0.4236	700.681	0.250
Resilence	0.8608	0.027	0.073	0.6214	0.063	0.110	0.7593	0.022	0.058	0.5459	0.050	0.081
pH	0.7511	0.057	0.010	0.4252	0.090	0.016	0.8254	0.069	0.012	0.5857	0.108	0.019
Color L	0.7655	0.649	0.011	0.5691	1.024	0.018	0.7525	0.839	0.014	0.4733	1.224	0.021
Color a*	0.7899	0.399	0.031	0.4752	0.713	0.056	0.9187	0.401	0.031	0.6300	0.684	0.053
Color b*	0.7997	0.467	0.065	0.3764	0.632	0.088	0.8463	0.311	0.043	0.5333	0.553	0.076
Moisture	0.8091	0.167	0.002	0.5515	0.210	0.003	0.8539	0.167	0.002	0.5859	0.198	0.002
Proteins	0.7972	0.198	0.009	0.4138	0.254	0.012	0.8451	0.182	0.008	0.6378	0.221	0.010
Lipids	0.7718	0.192	0.054	0.4918	0.258	0.073	0.8335	0.217	0.061	0.4466	0.264	0.074
Ash	0.7909	0.020	0.019	0.5706	0.035	0.032	0.8494	0.021	0.020	0.6957	0.043	0.039
Collagen	0.8398	0.012	0.026	0.5936	0.033	0.061	0.7096	0.017	0.038	0.4895	0.041	0.082
TBARs	0.8074	0.013	0.106	0.2138	0.022	0.179	0.8117	0.018	0.157	0.3476	0.028	0.214

of MRI-computational algorithms to classify chicken breast affected by the WS myopathy. As example, Fig. 4 shows the DT classification model based on the OPFTA algorithm. In this figure, red square on the leafs of the DT classification model shows the N group of samples, yellow ones represents the WS-M group of samples and green ones characterizes the WS-S group of samples.

Table 3 shows the statistical results on this classification technique: SENS >0.8, SPEC >0.9, PPV >0.8, NPV >0.9, error rate <0.2, fall-out rate <0.1, FDR <0.2, FOR <0.1, CSI >0.75, accuracy >0.9 and F1 score = 1.5–2 for the three batches, which indicate a very good classification according to Yerushalmy (1947). Besides, it is also noted that both computational algorithms obtained similar results, suggesting the possibility of application of J48 DT on GLCM or OPFTA features to classify chicken breasts with different WS affection degree. In fact, previous studies by applying DT on MRI computational characteristics from meat products have found accurate results. Caballero et al. (2016b) classified Iberian hams subjected to increasing post-salting processing time with an accuracy higher than 0.75. In other study, Iberian dry-cured shoulders were correctly classified as a function of the genotypes (Caballero et al., 2018c) and the feeding background of the pigs (Caballero et al., 2019) by means of DT. Moreover, DT was applied in order to monitor the hazards caused by the chemical substances (Van Asselt et al., 2018) and for evaluating the sensory attributes of processed meat products with natural compounds (Hung and Verbeke, 2018).

3.3. Prediction of physico-chemical parameters of chicken breast by means of MRI

Two predictive techniques of data mining (IR and MLR) were applied for determining physico-chemical parameters of chicken breast in a non-destructive way by MRI, testing the computational characteristics obtained by GLCM and OPFTA algorithms. In this way, four prediction equations were obtained for each physico-chemical characteristic, as a function of computational characteristics of both GLCM and OPFTA by means of MLR and IR. As example, Fig. 5 shows the prediction equations for the percentage of lipids and collagen of breast chicken when applying MLR. Table 4 shows values of R, MAE and WAPE of prediction equations for the physico-chemical characteristics of chicken breasts as a function of computational characteristics of GLCM and OPFTA by MLR and IR. Considering the data mining techniques, MLR reached higher correlation coefficients ($r > 0.75$ for all physico-chemical parameters) than IR. Moreover, lower MAE and WAPE values were obtained when applying MLR than IR. Thus, MLR should be selected for the prediction of physico-chemical parameters of chicken breast. This is in agreement with previous studies aimed to predict physico-chemical parameters of loins applying classical texture (Pérez-Palacios et al., 2017b) and fractal (Caballero et al., 2017) algorithms to analyze MRI images of loins. These authors pointed out the absence of lineal dependence between physico-chemical characteristics and computational features of MRI, because the use of MLR is indicated when there is not a high correlation between the data. Considering the computer vision algorithms, OPFTA achieved slightly better correlation coefficients than GLCM for thirteen of the seventeen physico-chemical characteristics. However, in the case of the error parameters (MAE and WAPE), GLCM achieved lower error values than OPFTA for twelve of the seventeen characteristics. Consequently, both computational algorithms may be used for the MRI analysis of chicken breast with prediction purposes.

Taking a step forward, Fig. 5 shows the adjustment for percentage of lipids (Fig. 5A) and collagen (Fig. 5B) between the values obtained by means of physico-chemical analysis and predicted as a function of the MRI computational features from GLCM and OPFTA and applying MLR. A similar performance for real values and those predicted with both GLCM and OPFTA can be observed. These two algorithms have been also compared in terms of computational time and complexity. Both methods take less than 50 ms/image (42 ms for GLCM and 47 ms for OPFTA, computed using a usual laptop INTEL i7-9750H, 2.6 GHz, 16 GB RAM). Besides, GLCM and OPFTA have similar computational complexity (O [n^2]) (Caballero et al., 2018b). Consequently, combinations of MLR with both GLCM and OPFTA may be used to determine physico-chemical characteristics of chicken breasts in a non-destructive way by MRI.

4. Conclusions

This is the first study to prove the capability of MRI-computer vision algorithms, as a non-destructive technique, to classify and predict quality characteristics of chicken breast affected by WS myopathy, evaluating the influence of the computational algorithms to analyze the MRI images and the techniques of data analysis on the classification and prediction results. Computational features from both texture (GLCM) and fractal (OPFTA) algorithms are useful to i) classify white striping chicken breast by means of different classification technique, Principal Component Analysis and Decision Tree, and ii) predict physico-chemical characteristics of these chicken breast with high accuracy, by means of Multiple Linear Regression. The objective and non-destructive

classification of WS conditions by degrees of severity in chicken breasts may be feasibly applied in large processing plants where the incidence of the myopathy is high and a quick decision-making is required for the fate of affected samples. In this regard, future work will be focused on reducing the time for image acquisition and developing automatic and on-line image analysis.

Author contribution

L. Carvalho contributed to perform the collection of samples, physico-chemical analysis, analyzed and interpreted data, contributed to write the manuscript and approved the final version. T. Pérez-Palacios contributed to the conceptualization of the original research. She verified the analytical methods, calculation and experiments, and supervised the project details. She took the lead in writing the manuscript and approved the final version. D. Caballero contributed to the conceptualization of the original research. He performed the MRI analysis, analyzed data and interpreted results. He took the lead in writing the manuscript and approved the final version. T. Antequera contributed to the conceptualization of the original research and to the interpretation of results. She contributed to write the manuscript and approved the final version. M. S. Madruga contributed to the project funding and interpretation of the results. She contributing to writing the manuscript by providing critical comments and approved the final version. M. Estévez contributed to project funding and the conceptualization of the original research. He supervised the project details. He contributed to writing the manuscript and approved the final version.

Declaration of competing interest

The authors declare that they have no known competing financial interests or personal relationships that could have appeared to influence the work reported in this paper.

Acknowledgements

The authors acknowledge the following funders: #1 "CNPq – Brazilian National Council for Scientific and Technological Development" (grant number 430832/2016-8); #2 "Government of Extremadura (*Consejería de Economía e Infraestructuras*) and the European Union (Fondo Europeo de Desarrollo Regional, "*Una manera de hacer Europa*")" for the grant numbers IB16043 and GR18104; and #3 "Government of Extremadura" for Daniel Caballero's postdoctoral grant, number PO17017.

References

Aggarwal, N., Agrawal, R.K., 2012. First and second order statistics features for classification of magnetic resonance brain images. J. Signal Inf. Process. 3, 574–580.
Alnahhas, N., Berri, C., Chabault, M., Chartrin, P., Boulay, M., Bourin, M.C., Le Bihan-Duval, E., 2016. Genetic parameters of white striping in relation to body weight, carcass composition, and meat quality traits in two broiler lines divergently selected for the ultimate pH of the pectoralis major muscle. BMC Genet. 17 (1), 61.
Antequera, T., Caro, A., Rodríguez, P.G., Pérez, T., 2007. Monitoring the ripening process of Iberian ham by computer vision on magnetic resonance imaging. Meat Sci. 76 (3), 561–567.
Armenteros, M., Heinonen, M., Ollilainen, V., Toldrá, F., Estévez, M., 2009. Analysis of protein carbonyls in meat products by using the DNPH-method, fluorescence spectroscopy and liquid chromatography-electrospray ionisation-mass spectrometry (LC-ESI-MS). Meat Sci. 83 (1), 104–112.
Association of Official Analytical Chemistry (A.O.A.C), 2000. Official Methods of Análisis of AOAC International, s. 1. AOAC International, Gaithersburg, Maryland, U.S.A, p. 2.
Ávila, M.M., Caballero, D., Durán, M.L., Caro, A., Pérez-Palacios, T., Antequera, T., 2015. Including 3D-textures in a computer visión system to analyze quality traits of loin. Lect. Notes Comput. Sci. 9163, 456–465.
Ávila, M.M., Durán, M.L., Caballero, D., Antequera, T., Pérez-Palacios, T., Cernadas, E., Fernández-Delgado, M., 2019. Magnetic Resonance Imaging, texture analysis and regression techniques to non-destructively predict the quality characteristics of meat pieces. Eng. Appl. Artif. Intell. 82, 110–125.
Baldi, G., Soglia, F., Mazzoni, M., Sirri, F., Canonico, L., Babini, E., Laghi, L., Cavani, C., Petracci, M., 2018. Implications of white striping and spaghetti meat abnormalities on meat quality and histological features in broilers. Animal 12 (1), 164–173.
Barlow, R.E., Bartholomew, D., Bremmer, J.M., Brunk, H.D., 1972. Statistic Inference under Order Restriction: the Theory and Application of Isotonic Regression. Wiley, New York, New York, U.S.A.
Bonny, J.M., Laurent, W., Labas, R., Taylor, R., Berge, P., Renou, J.P., 2000. Magnetic Resonance imaging of connective tissue: a non-destructive method for characterising muscle structure. J. Sci. Food Agric. 81, 337–341.
Bro, R., Smilde, A.K., 2014. Principal component analysis. Analytical Methods 6, 2812–2831.
Caballero, D., Caro, A., Antequera, T., Pérez-Palacios, T., 2016a. Non-destructive analysis of loin by magnetic resonance imaging and fractal. IX International Symposium on the Mediterranean Pig. Portalegre, Portugal.
Caballero, D., Caro, A., Rodríguez, P.G., Durán, M.L., Ávila, M.M., Palacios, R., Antequera, T., Pérez-Palacios, T., 2016b. Modeling salt diffusion in Iberian ham by applying MRI and data mining. J. Food Eng. 189, 115–122.
Caballero, D., Pérez-Palacios, T., Caro, A., Amigo, J.M., Ersboll, B.K., Dahl, A.B., Antequera, T., 2017. Prediction of pork quality parameters by applying fractals and data mining on MRI. Food Res. Int. 99, 739–747.
Caballero, D., Antequera, T., Caro, A., Amigo, J.M., Ersboll, B.K., Dahl, A.B., Pérez-Palacios, T., 2018a. Analysis of MRI by fractals for prediction of sensory attributes: a case study in loin. J. Food Eng. 227, 1–10.
Caballero, D., Caro, A., Dahl, A.B., Ersboll, B.K., Amigo, J.M., Pérez-Palacios, T., Antequera, T., 2018b. Comparison of different image analysis algorithms on MRI to predict physico-chemical and sensory attributes of loin. Chemometr. Intell. Lab. Syst. 180, 54–63.
Caballero, D., Asensio, M., Fernández, C., Martín, N., Silva, A., 2018c. Classifying different Iberian pig genetic lines by applying chemical-instrumental parameters of dry-cured Iberian shoulders. J. Food Sci. Technol. 55 (11), 4589–4599.
Caballero, D., Asensio, M., Fernández, C., Reina, R., García-Casco, J., Martín, N., Silva, A., 2019. Chemical-instrumental-sensory traits and data mining for classifying dry-cured Iberian shoulders from pigs with different diets. Journal of Food Measurement and Characterization 13, 2935–2950.
Carvalho, L., Oliveira, M.E., Freitas, A.S., Sousa-Neto, A.C., Ida, E.I., Shimokomaki, M., Madruga, M., 2018. Further evidence for the existence of broiler chicken PFN (pale, firm, non-exudative) and PSE (pale, soft, exudative) meat in Brazilian commercial flocks. Food Sci. Technol. 38 (4), 704–710.
Cernadas, E., Antequera, T., Rodríguez, P.G., Durán, M.L., Gallardo, R., Villa, D., 2001. Magnetic resonance imaging to classify loin from iberian pigs. In: Webb, G.A., Belton, P.S., Gil, A.M., Delgadillo, I. (Eds.), Magnetic Resonance in Food Science: A View to the Future, T. he royal society of Chemistry, Cambridge, United Kingom, pp. 239–245.
Colton, T., 1974. Statistical in Medicine. Little Brown and Co., New York, New York, U.S.A.
Davanel, A., Seigneurin, F., Collewet, G., Remignon, H., 2000. Estimation of poultry breast meat yield: magnetic resonance imaging as a tool to improve the positioning of ultrasonic scanners. Meat Sci. 56, 153–158.
Demsar, J., 2006. Statistical comparison of classifiers over multiple data sets. J. Mach. Learn. Res. 7, 1–30.
Dietterich, T., 1998. Approximate statistical tests for comparing supervised classification learning algorithms. Neural Comput. 10 (7), 1895–1923.
Ebrahimnejad, H., Ebrahimnejad, H., Salajegheh, A., Barghi, H., 2018. Use of magnetic resonance imaging in food quality control: a review. Journal of Biomedical Physics and Engineering 8 (1), 127–132.
Folch, J., Lees, M., Sloane-Stanley, G.H., 1957. A simple method for the isolation and purification of total lipids from animal tissues. J. Biol. Chem. 226 (1), 497–509.
Ganhao, R., Estévez, M., Morcuende, D., 2011. Suitability of the TBA method for assessing lipid oxidation in meat system with added phenolic-rich material. Food Chem. 126 (2), 772–778.
Geronimo, B.C., Mastelini, S.M., Carvalho, R.H., Barbon Júnior, S., Barbin, D.F., Shimokomaki, M., Ida, E.I., 2019. Computer vision system and near-infrared spectroscopy for identification and classification of chicken with wooden breast, and physicochemical and technological characterization. Infrared Phys. Technol. 96, 303–310.
Hand, D.J., 2012. Assessing the performance of classification methods. Int. Stat. Rev. 80 (3), 400–414.
Haralick, R.M., Shapiro, L.G., 1993. Computer and Robot Vision. Addison-Wesley, Chicago.
Hastie, T., Tibshirani, R., Friedman, J., 2001. The Elements of Statistical Learning: Data Mining Inference and Prediction. Springer-Verlag., New York, New York, U.S.A.
Hung, Y., Verbeke, W., 2018. Sensory attributes shaping consumers' willingness-to-pay for newly developed processed meat products with natural compounds and a reduced level of nitrite. Food Qual. Prefer. 70, 21–31.
Jiang, H., Yoon, S.C., Zhuang, H., Wang, W., Li, Y., Yang, Y., 2019. Integration of spectral and textural features of visible and near-infrared hyperspectral imaging for differentiating between normal. Spectrochemical Acta Part A Molecular and Biomolecular Spectroscopy 213, 118–126.
Kato, T., Mastelini, S.M., Campos, G.F.C., Borbon, A.P.A.C., Prudencio, S.H., Shimokomaki, M., Soares, A.L., Borbon Jr., S., 2019. White striping degree assessment using computer vision system and consumer acceptance test. Asian-Australas. J. Anim. Sci. 32 (7), 1015–1026.
Kira, K., Rendell, L.A., 1992. A practical approach to feature selection. IX International Conference on Machine Learning. Aberdeen, United Kingdom.

Kuttappan, V.A., Brewer, V.B., Apple, J.K., Waldroup, P.W., Owens, C.M., 2012. Influence of growth rate on the occurrence of white striping in broiler breast fillets. Poultry Sci. 91 (10), 2677–2685.
Kuttappan, V.A., Shivaprasad, H.L., Shaw, D.P., Valentine, B.A., Hagis, B.M., Clark, F.D., McKee, S.R., Owens, C.M., 2013. Pathological changes associated with white striping in broiler breast muscle. Poultry Sci. 92, 331–338.
Lufkin, R.B., 1998. The MRI Manual. Saint Louis. Mosby-Year Book, Missouri, U.S.A.
Mandelbrot, B.B., 1982. The Fractal Geometry of Nature. W.H. Freeman and Co, New York, New York, U.S.A.
Molano, R., Rodríguez, P.G., Caro, A., Durán, M.L., 2012. Finding the largest area rectangle of arbitrary orientation in a closed contour. Appl. Math. Comput. 218, 9866–9874.
Pérez-Palacios, T., Antequera, T., Durán, M.L., Caro, A., Rodríguez, P.G., Ruiz, J., 2010. MRI-based análisis, lipid composition and sensory traits for studying Iberian dry-cured hams from pigs fed with different diets. Food Res. Int. 43, 248–254.
Pérez-Palacios, T., Antequera, T., Durán, M.L., Caro, A., Rodríguez, P.G., Palacios, R., 2011. MRI-based analysis of feeding background effect on fresh Iberian ham. Food Chem. 126 (3), 1366–1372.
Pérez-Palacios, T., Caballero, D., Caro, A., Rodríguez, P.G., Antequera, T., 2014. Applying data mining and Computer Vision Techniques to MRI to estimate quality traits in Iberian hams. J. Food Eng. 131, 82–88.
Pérez-Palacios, T., Caballero, D., Bravo, S., Mir-Bel, J., Antequera, T., 2017a. Effect of cooking conditions on quality characteristics of confit cod: prediction by MRI. Int. J. Food Eng. 13 (8), 20160311.
Pérez-Palacios, T., Caballero, D., Antequera, T., Durán, M.L., Ávila, A., Caro, A., 2017b. Optimization of mri acquisition and texture analysis to predict physico-chemical parameters of loins by data mining. Food Bioprocess Technol. 10, 750–758.
Petracci, M., Cavani, C., 2012. Muscle growth and poultry meat quality issues. Nutrients 4, 1–12.
Petracci, M., Mudalal, S., Bonfiglio, A., Cavani, C., 2013. Occurrence of white striping under commercial conditions and its impact on breast meat quality in broiler chickens. Poultry Sci. 92 (6), 1670–1675.
Petracci, M., Soglia, F., Madruga, M., Carvalho, L., Ida, E., Estévez, M., 2019. Wooden-breast, white striping, and spaghetti meat: causes, consequences and consumer perception of emerging broiler meat abnormalities. Compr. Rev. Food Sci. Food Saf. 18 (2), 565–583.
Safavian, R., Landgrebe, D., 1991. A survey of decision tree classifier methodology. IEEE Transactions on Systems, Man and Cybernetics 21 (3), 660–674.
Soglia, F., Laghi, L., Canonico, L., Cavani, C., Petracci, M., 2016. Functional property issues in broiler breast meat related to emerging muscle abnormalities. Food Res. Int. 89, 1071–1076.
Torres, J.P., Ávila, M., Caro, A., Pérez-Palacios, T., Caballero, D., 2019. Non-destructively prediction of quality parameters of dry-cured Iberian ham by applying computer vision and low-field MRI. Lect. Notes Comput. Sci. 11867, 498–507.
Toussiant, C., Fauconneau, B., Medale, F., Collewet, G., Akoka, S., Haffray, P., Davenel, A., 2005. Description of the heterogeneity of lipid distribution in the flesh of brown trout (Salmo Trutta) by MR imaging. Aquaculture 243, 255–267.
Traffano-Schiffo, M.V., Castro-Giraldez, M., Colom, R.J., Fito, P.J., 2017. Development of a spectrophotometric system to detect white striping physiopathy in whole chicken carcasses. Sensors 17 (5), 1024.
Van asselt, E.D., Noordam, M.Y., Pikkemaat, M.G., Dorgelo, F.O., 2018. Risk-based monitoring of chemical substances in food: prioritization by decision trees. Food Contr. 93, 112–120.
Witten, I.H., Frank, E., 2005. In: Morgan-Kauffman (Ed.), Data Mining: Practical Machine Learning Tools and Techniques with Java Implementations (San Francisco, California, U.S.A).
Wu, X., Kumar, V., Ross-Quinlan, J., Ghosh, J., Yang, Q., Motoda, H., McLachlan, G.J., Ng, A., Liu, B., Yu, P.S., Zhou, Z.H., Steinbach, M., Hand, D.J., Steinberg, D., 2008. Top 10 algorithms in data mining. Knowl. Inf. Syst. 14, 1–37.
Xiong, Z., Sun, D.W., Pu, H., Gao, W., Dai, Q., 2017. Applications of emerging imaging techniques for meat quality and safety detection and evaluation: a review. Crit. Rev. Food Sci. Nutr. 57 (4), 755–768.
Yerushalmy, J., 1947. Statistical problems in assessing methods of medical diagnosis with special reference to x-ray techniques. Publ. Health Rep. 62 (2), 1432–1439.